CHAPTER 3

Optical Components Based On Dynamic Liquid-Liquid Interfaces

Sindy K.Y. Tang and George M. Whitesides

Department of Chemistry and Chemical Biology, Harvard University

3-1 Introduction

This chapter describes optical components based on dynamic liquid-liquid (L^2) interfaces between liquids with different optical properties (such as index of refraction) in microfluidic systems. Devices with optical interfaces formed by liquids have characteristics that are quite different from solid-gas and solid-liquid systems commonly used in conventional optics.

L^2 systems have four attractive characteristics.

1. It is simple to reconfigure the properties and functions of L^2 systems in real time by adjusting the compositions of the liquids, and their rates of flow.
2. Unlike their solid-state counterparts, polishing or high-precision microfabrication is not necessary to obtain smooth optical interfaces for L^2 devices: the L^2 interfaces are intrinsically smooth as a result of laminar flow that is characteristic of microfluidic systems.

3. It is straightforward to obtain a graded profile of refractive index in L^2 systems by taking advantage of diffusion between miscible liquids possessing different refractive indices.
4. Since the L^2 devices are formed inside a microfluidic channel, the manipulation of the liquids used for optics in microchannels is the same as that of liquids used for other purposes (separations, reagent storage, sample preparation, etc.). It is thus possible to design and cofabricate the channels for the optical parts of integrated system, and for other parts simultaneously. This feature facilitates integration and prealignment of L^2 devices to the relevant components on the same microfluidic platform.

This chapter has two objectives:

1. To discuss the basic construction of L^2 devices, and the characteristics of dynamic L^2 interfaces formed between laminar streams in microchannels; and
2. To give examples of optofluidic devices—L^2 waveguides, L^2 lenses, L^2 light sources, and bubble diffraction grating—to demonstrate the design and operation of these devices.

3-2 Basic Design and Construction of Liquid-Liquid (L^2) Devices

Typically, L^2 devices consist of multiple streams of liquids possessing different optical properties (such as refractive indices) coflowing in a single microchannel. Figure 3-1 shows a representative design of a L^2 device. It consists of multiple inlets for different liquids to flow into a

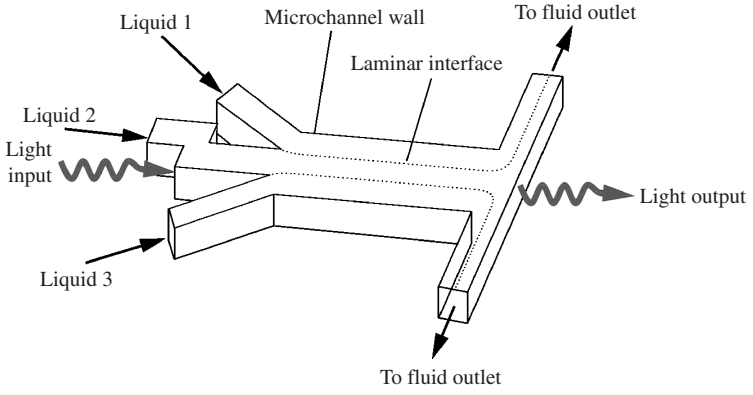

Figure 3-1 Schematic representation of the typical design of a L^2 device.

main channel. Depending on the application, this main channel can have different geometries (a straight channel of uniform width is shown in Fig. 3-1). To form and maintain the L^2 interface, liquids are injected continuously into the channel. The rate of flow is sufficiently small such that the flow is laminar.

To couple light into and out of the L^2 devices, external lenses can be used to focus light from an off-chip light source into the microchannel across the polydimethylsiloxane (PDMS) wall. Alternatively, light can be coupled into an optical fiber, which is then inserted into the PDMS device through appropriate ports. The use of fibers facilitates optical alignment between external light sources, or detectors, and the microfluidic channel, and allows substantial flexibility in system design. It is therefore a common way of introducing light into L^2 devices.

AU: Please consider expanding at the first occurrence.

Ports for insertion of optical fiber (Fig. 3-2) are often included in the design of L^2 devices [1]; they are fabricated at the same time as the rest of the microchannels. Light introduced through these inserted fibers is in the same plane of the microchannels. The port for the

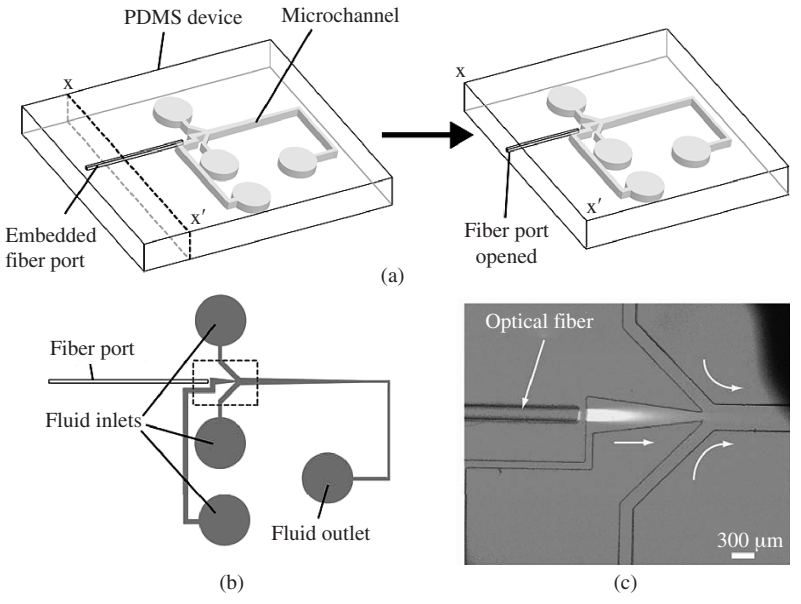

Figure 3-2 (a) Diagram of the sealed channel. The dotted line (x – x') depicts a typical location for cutting the sealed channel to expose the inlet for the optical fiber. (b) Top-down view of the schematic diagram of the microfluidic channel. (c) Optical micrograph of the inlet portion of the channel inside the dashed lines in (b) after the insertion of an optical fiber. The light from the optical fiber is from a fiber-coupled deuterium lamp. The channel is filled with a solution of fluorescein (1 mM). The bright area to the right of the fiber is the fluorescence of the fluorescein, and it shows the path of the light from the fiber into the fluid-filled channel. The small arrows depict the direction of the flow of the guiding-liquid and cladding-liquid streams. (*Adapted from Ref. 1.*)

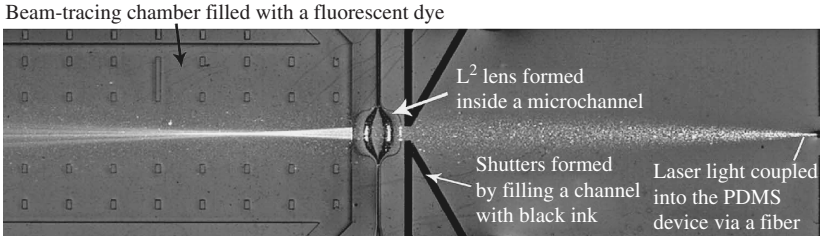

FIGURE 3-3 Bright-field image of beam-tracing chamber showing the optical path behind the L^2 lens. The laser beam from the fiber is visible in front of the aperture because PDMS contains nanoparticles of silica that scatter light. The focused beam in the beam-tracing chamber is visualized by the fluorescence of a rhodamine dye filling the chamber. (*Adapted from Ref. 2.*)

optical fiber is usually left sealed in the PDMS during the fabrication of the device; this port is opened later by cutting the back part of the sealed channels with a razor blade (Fig. 3-2A; x–x′). This cut opens a channel at the edge of the PDMS that has the dimensions of the fiber (width × height ~ 100 μm × 100 μm). The open channel accommodating the optical fiber ends at a distance from the fluidic channel, and is isolated from the fluids. Depending on the application, this distance varies from a few tens of microns (for L^2 waveguides) to a few millimeters (for L^2 lens). The optical fiber is then manually inserted into this open channel. Index-matching liquids can be applied to fill any air gap between PDMS and the optical fiber. The center of the fiber channel is collinear with the center of the microfluidic channel.

To visualize the propagation of light inside the PDMS device, one can introduce fluorescent dyes in a chamber fabricated in the optical path [2]. This "beam-tracing" chamber is used for characterization of the focal distance and the quality of the focused beam of the L^2 lens, for example (Fig. 3-3). The solution of dye fluoresces only in regions where there was optical illumination. The concentration of the dye solution should be sufficiently low such that the incident light could propagate through the beam-tracing chamber without being significantly attenuated or absorbed. To avoid photobleaching of the dye during the experiment, the intensity of the incident light should also be sufficiently low; alternatively, new dye solution can be injected continuously to replace the photobleached dyes.

3-3 Index of Refraction of Common Liquids

Contrast of refractive index in liquids can be provided in several ways, including

1. Different liquids. A wide range of common liquids are transparent in the visible region of the spectrum, and have refractive indices ranging from 1.28 to 1.75 [3]. Table 3-1 lists the refractive indices of some common solvents.

Name	Refractive index n_d	NFPA*	Compatibility with PDMS†
Methylene iodide	1.749	H3; F1; R0	No
1,2-Diiodobenzene	1.718	H1; F1; R1	(not available)
1-Iodonaphthalene	1.701	H2; F1; R0	(not available)
Benzothiazole	1.642	H2; F0; R0	Yes
Carbon disulfide	1.627	H3; F4; R0	(not available)
1-Methylnaphthalene	1.618	H1; F2; R1	(not available)
Bromoform	1.596	H3; F0; R0	No
Thiophenol	1.588	H4; F2; R0	Yes
Nitrobenzene	1.550	H3; F2; R1	Yes
Benzaldehyde	1.544	H2; F2; R0	Yes
Benzyl alcohol	1.538	H1; F1; R0	Yes
Thiophene	1.526	H2; F3; R0	(not available)
Dimethyl sulfoxide	1.479	H1; F1; R0	Yes
Formamide	1.447	H2; F1; R0	Yes
N,N-Dimethylacetamide	1.438	H2; F2; R0	Yes
Ethylene glycol	1.429	H1; F1; R0	Yes
Propylene carbonate	1.422	H1; F1; R0	Yes
Ethanol	1.359	H0; F3; R0	Yes
Water	1.333	H0; F0; R0	Yes
Methanol	1.328	H1; F3; R0	Yes
2,2,2-Trifluoroethanol	1.300	H2; F3; R0	Yes

* The National Fire Protection Agency (NFPA) hazard identification system: H, F, R represents health, flammability, and reactivityrespectively. The number ratings range from 0 to 4. A rating of 0 represents essentially no hazard; a rating of 4 indicates extreme danger. http://www.ssrl.slac.stanford.edu/safety/nfpa_hazard_class.html.

† We define a liquid to be compatible with PDMS if the swelling ratio (defined as D/D_0, where D is the length of the solid PDMS in the solvent and D_0 is the length of the dry, solid PDMS) is less than 1.1 after a solid piece of PDMS is placed in a solvent for 24 h. Details regarding individual solvent's compatibility with PDMS can be found in Ref. [7].
(Extracted from S. K. Y. Tang, C. A. Stan, and G. M. Whitesides, "Dynamically Reconfigurable Liquid-Core Liquid-Cladding Lens in a Microfluidic Channel," *Lab Chip*, 8, (2008), 395–401.)

TABLE 3-1 Refractive Index, Hazard Codes, and Compatibility with PDMS of Selected Liquids

2. Different concentrations of solutes in aqueous or organic solutions. Table 3-2 shows the variation of refractive index with concentration of aqueous solutions of calcium chloride and sucrose respectively.
3. A single homogeneous liquid with a difference in temperature. The thermo-optical coefficient (the change in refractive index with change in temperature) is typically around $1 \times 10^{-4}°C^{-1}$ for common liquids between 10°C and 80°C [4]. Water, for example, has an index $n_d = 1.3325$ at 10°C and an index $n_d = 1.3235$ at 75°C.
4. A suspension of dielectric nanoparticles, for example, a suspension of polystyrene particles in water (diameter = 160 nm, volume fraction = 0.25%) [5].
5. Liquids with refractive indices modulated by external forces such as electric fields (e.g., liquid crystals), and magnetic fields (e.g., magnetic fluid such as water-based Fe_3O_4 is reported to have an increase in refractive index $\Delta n = 0.005$ when the magnetic field increased from 25 to 300 Oe [6].

The choice of liquids to provide the contrast in refractive index depends on the application. The refractive index of organic solvents can go up to 1.75, but they may be toxic and incompatible with PDMS. The use of a single homogeneous liquid at different temperatures

Calcium chloride solution		Sucrose solution	
% by mass	Refractive index	% by mass	Refractive index
1.00	1.3354	1.00	1.3344
5.00	1.3451	10.00	1.3478
10.00	1.3575	20.00	1.3639
15.00	1.3704	30.00	1.3812
20.00	1.3839	40.00	1.3999
26.00	1.4008	50.00	1.4201
30.00	1.4124	60.00	1.4419
34.00	1.4242	70.00	1.4654
38.00	1.4361	80.00	1.4906
40.00	1.4420	84.00	1.5010

(Extracted from David R. Lide, Editor in chief, "Density, Refractive Index, Freezing Point Depression, and Viscosity of Aqueous Solutions," Handbook of Chemistry and Physics, 77th ed, CRC , 8-56–8-78,

TABLE 3-2 Refractive Index of Aqueous Solutions of Calcium Chloride and Sucrose at Different Concentrations

simplifies recycling, and facilitates closed-loop operation. Thermal diffusivity in liquids is typically two orders of magnitude higher than mass diffusivity of solute ions [4], however. A much higher rate of flow is therefore necessary to maintain the contrast in refractive index across the L^2 interface.

3-4 Dynamic Liquid-Liquid Interfaces in Microfluidic Systems

The interface between laminar streams in microfluidic systems is at dynamic steady state: continuous flow is required to maintain the interface between the streams. The use of this dynamic interface as part of an optical component has advantages and disadvantages, as discussed next.

3-4-1 L^2 Interfaces Are Reconfigurable in Real Time

Liquids can be replaced and/or replenished continuously in L^2 systems. This capability for replacement allows injection of liquids with different properties (e.g., index of refraction, absorption, and fluorescence) to tune the optical output of the system in real time. The ability to replenish liquids makes photobleaching and related phenomena relatively unimportant, since the component that is bleached is replaced continuously. This latter feature is especially important for the operation of microfluidic dye lasers—without a continuous replacement of solutions of dye, the lasing action would stop in a few seconds when the dye is photobleached. The disadvantage here is the need for constant supply of liquids. Microfluidic systems allow economical use of solutions and reagents, however; the consumption of fluids is therefore limited.

Another way to reconfigure the L^2 interface is by manipulating the flow conditions. The L^2 interface is deformable: it is possible to change the position or the shape of the liquid-liquid interface, and therefore the path of light inside the optofluidic devices by changing rates of flow (and other properties such as viscosity) of the fluids. Changing the relative volumetric rates of flow between the streams of liquids changes the position or the shape of the L^2 interface. The L^2 lens, for example, can take up shapes varying from biconvex to plano-convex to meniscus simply by changing the relative rates of flow between the core and cladding streams.

The switching time of liquids in microchannels is on the order of seconds. This time scale is limited by the time required for mass transport of liquids in the microfluidic system. This value is much longer than that in conventional optical systems. Nevertheless, the liquid-liquid system should meet the demands of applications that do not require fast switching, such as optical sensing and bioassays.

3-4-2 L^2 Interfaces Are Smooth

Unlike their solid-state counterparts, polishing or high-precision fabrication is not necessary to obtain smooth optical surfaces in L^2 devices. Because of their small length scale, L^2 devices operate in the low Reynolds number regime, and the flow is laminar (i.e., nonturbulent). Fluid flows at low Reynolds number generate an intrinsically optically smooth interface between streams of liquids. Small irregularities in the solid walls of the channels (having roughness of r) do not propagate into the liquid interfaces, as long as the width of the flowing streams is larger than $2r$ [8]. Figure 3-4 shows that the walls of the PDMS microfluidic channel are relatively rough (there is obvious roughness with dimensions > 5 μm). The L^2 interface, as viewed in this image, is still smooth. The generation of optically smooth interface in this rough channel is possible due to laminar flow of the streams of liquids. When the roughness is less than 5% of the total width of the channel, its effect is negligible on the interfaces between streams. It implies that it is possible to use low-precision fabrication to make the microfluidic channels, and still produce high-quality optical fluidic interfaces.

By introducing a liquid with refractive index matched to that of PDMS ($n_d = 1.41$) to "line" the channel, it is possible to reduce losses due to scattering of light that passes through the side wall of the channel. In the case of the L^2 lens, for example, the use of a mixture of 73.5% ethylene glycol ($n_d = 1.43$) and 26.5% ethanol ($n_d = 1.36$) (effective index $n_{deff} = 1.41$) as the cladding liquid reduced undesired scattering of light across the PDMS-liquid interface, and improved the quality of the focused beam (Fig. 3-10b and 3-10c). Other mixtures of liquids or solutions of different salt concentrations should also work.

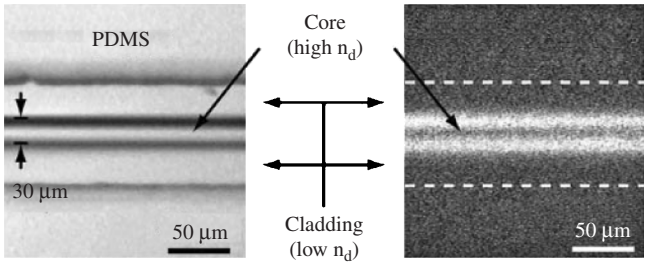

Figure 3-4 (a) Optical micrograph of the L2 waveguide. The core fluid was dyed to aid visualization. (b) Fluorescence micrograph of the same region of the channel as in A. The visible fluorescence signal has been produced by excitation with a broadband deuterium, fiber-coupled light source leaking into the evanescent field from the core of the waveguide. The dotted lines indicate the location of the walls of the microchannel. (*Adapted from Ref. 1.*)

3-4-3 L^2 Interface between Miscible Liquids Is Diffuse

The L^2 interface between miscible liquids is diffuse—it is a gradient of chemical/physical composition and refractive indices. Diffusion of molecules or ions between different liquids broadens the interface between the streams. This diffusion creates a graded profile of refractive index across the interface. This feature is attractive for applications that require a gradient of refractive index, such as GRIN lenses, and diffusive splitters. This graded profile is more difficult to generate, and almost impossible to modify in solid-state systems.

Diffusion, when sufficiently extended, flattens the contrast in chemical/physical composition (e.g., salt concentration, temperature) of the respective fluids, and therefore the contrast in the refractive index that defines the fluidic-optical interface. As described in Chap. 1, for solute ions flowing through a channel with width w = 100 μm at velocity v = 100 μms^{-1}, it would take only 5 s for the ions to diffuse across the width of the entire channel. That is, within 500 μm down the channel, the contrast in concentration and refractive index will be flattened. The use of a more viscous liquid, or a higher rate of flow of liquids, can mitigate this effect. Increasing the rate of flow reduces the residence time of the liquids inside the channel, and therefore reduces diffusive broadening for the same length of the channel. Figure 3-5 shows the simulations for the profile of refractive index at different rates of flow. In principle, the use of immiscible liquids can eliminate diffusion completely, but different wetting properties of the liquids on the PDMS wall and surface tension between the liquids (leading to droplet formation) can complicate the flow and make the manipulation of the L^2 interface more difficult.

3-5 Liquid-Liquid (L^2) Optical Devices

3-5-1 L^2 Waveguides

Design and Construction

L^2 waveguides consist of two streams of liquids with lower refractive index (the cladding), sandwiching a stream of liquid with higher refractive index (the core) flowing in a microchannel [1] (Fig. 3-6). In principle, any liquid that does not swell PDMS [7] can be used in L^2 waveguides, as long as the contrast in index of refraction between the core and the cladding streams are large enough to sustain the propagation of light. In much of our work, we used a 5-M aqueous solution of calcium chloride (n_d = 1.45) as the core liquid, and water as the cladding (n_d = 1.33).

To introduce light into the device, an optical fiber is inserted into the PDMS device through a fiber port fabricated at the end of the channel. The guided light exits the L^2 waveguide when the core fluid is forced to turn by 90° with a radius of ~ 0.5 mm (much less than the

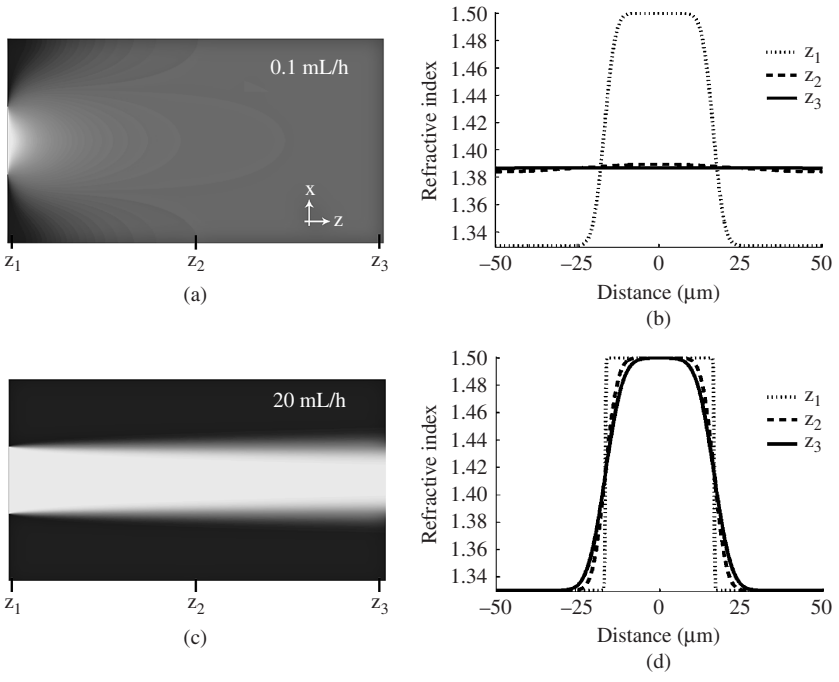

Figure 3-5 Simulated two-dimensional (*xz*) distributions of refractive index in a 5 mm long waveguide formed by water at total rates of flow of (A) 0.1 mL/h and (c) 20 mL/h. The refractive index of the injected core liquid n_{core} is 1.50, and is represented in white. The refractive index of the injected cladding liquid $n_{cladding}$ is 1.33, and is represented in black. Plot of the refractive index as a function of distance from the center of the waveguide in the transverse (*x*) direction for three longitudinal positions (z_1, z_2, and z_3) at total rates of flow of (b) 0.1 mL/h and (d) 20 mL/h. In this simulation, the width, height, and length of the channel are 100 μm, 100 μm, and 5 mm respectively; the diffusivity is 10^{-9} m^2/s, and the viscosity is 8.90×10^{-4} Pa·s.

critical radius) [9]. The output of the L^2 waveguide can then be imaged and analyzed through an optically transparent window (Fig. 3-6) by using a microscope objective and a charge-coupled device, or through an additional inlet for an optical fiber at the end of the channel coupled to a photodetector.

Characterization

By controlling the relative rates of flow of the core and cladding liquids, it is possible to change the width of the core stream to achieve both single- and multimode guiding. Decreasing the ratio of flow rates of the core to the cladding streams decreases the core size from more than 100 μm to less than 10 μm, and thus switches the guiding from multi- to single-mode. At a rate of flow of 10 μL/min, the distance at which the L^2 waveguide can operate before complete diffusive mixing homogenizes the liquids is ~ 5 mm. This length scale is limited by diffusive broadening of the interface between streams, which decreases the contrast in refractive index between the core and the cladding.

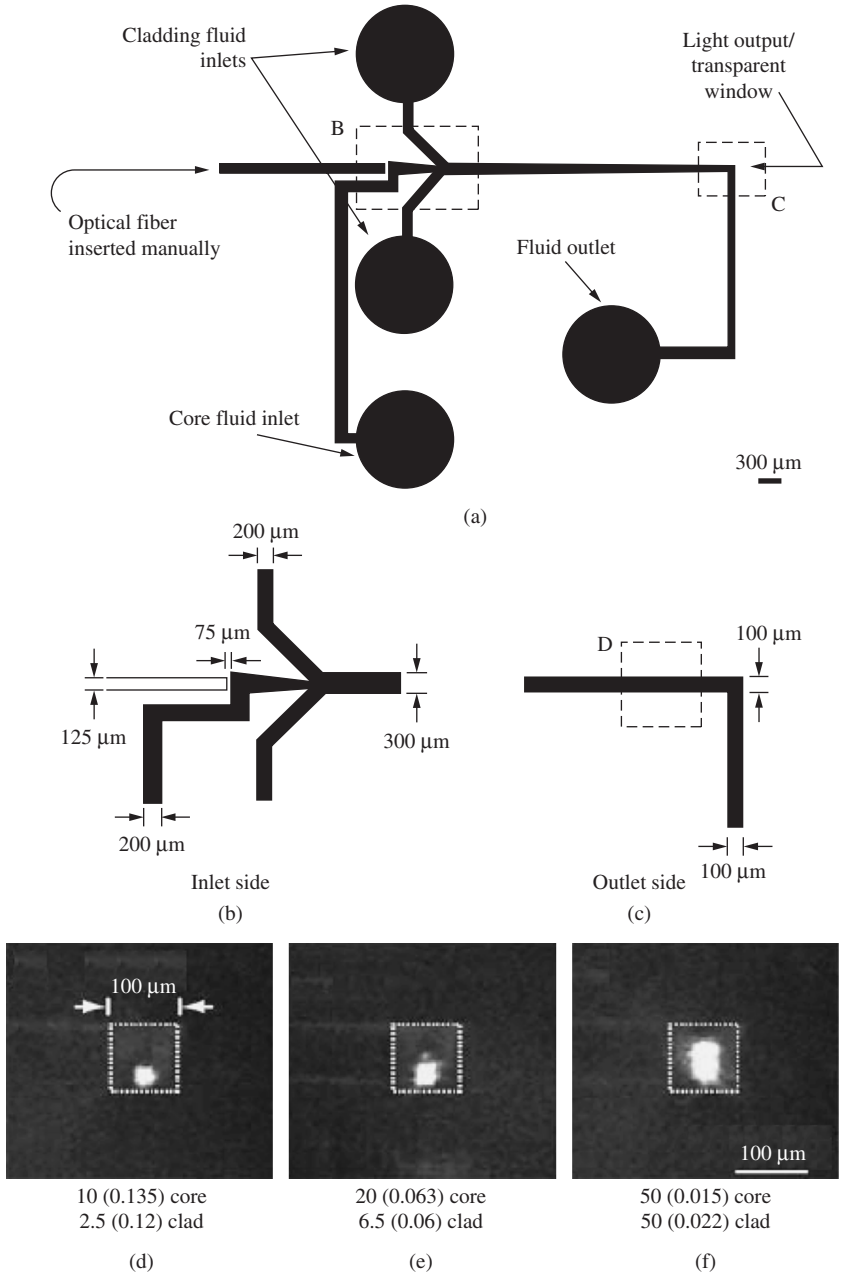

FIGURE 3-6 (a) Diagram of the design of a microfluidic channel used in these experiments. (b–c) Detailed diagrams of the regions of the microfluidic channel in A highlighted by dashed box. (d–f) Optical micrographs of the cross section of the outlet of the microfluidic channel viewed through the transparent window. The dashed box shows the location of the cross section of the microfluidic channel. The rates of flow (uL/min) (and the residence time in seconds) of the core and the cladding (clad) are listed. The guided light was from a fiber-coupled laser with $\lambda = 780$ nm. (*Adapted from Ref. 1.*)

This unfavorable effect can be partially circumvented, however, by using a higher rate of flow as mentioned in the previous section.

The loss in the intensity of guided light in L^2 waveguides is around 0.1 dB/cm. The efficiency of coupling light from the L^2 waveguide into a multimode optical fiber (step-index fiber, numerical aperture = 0.22, core diameter = 105 μm, cladding diameter = 125 μm) is ~ 40%. Light exiting the L^2 waveguide remains polarized in the input direction to ~ 100:1; this ratio is indistinguishable from the light in the input fiber.

Complex Devices Derived from L^2 Waveguides

Based on the L^2 waveguide configuration, we have developed other functional optical devices in microfluidic systems (Fig. 3-7).

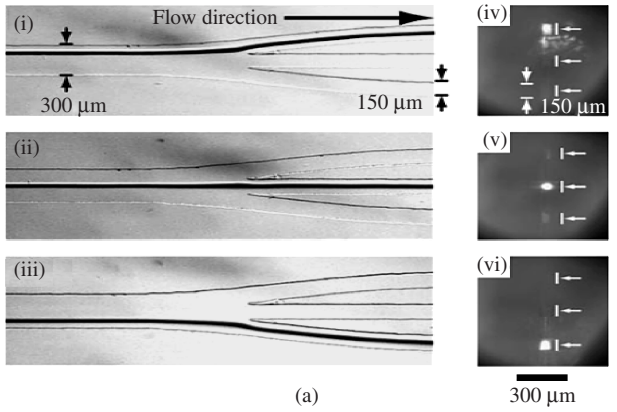

Figure 3-7 (a) *Optical switch*. (i)–(iii) Optical micrograph of the top view of the microfluidic channels. Dye in the core fluid makes it easily imaged; the dye is omitted in use. (iv)–(vi) Optical micrograph of the cross section of the end of the channel showing light exiting the L^2 waveguides. The white arrows and lines represent the location of the ends of the branches of the microfluidic channel. (b) *Evanescent coupler*. Plot of the ratio of the intensity of the light emitted from the coupled guide (ICG) and the illuminated guide (IIG). (Insets) Shown are optical micrographs of the cross section of the output of the microfluidic channels viewed through the transparent window. (c) (i) Plot of the profile of the intensity of light output as a function of distance from the center of the channel. The light (λ = 780 nm) was coupled into the L^2 waveguide from a single-mode optical fiber. The rate of flow of the core fluids was 2.5 μL/min, of the central cladding fluids was 5 μL/min, and of the outer cladding fluids was 10 μL/min. (Inset) Optical micrograph of light exiting the microfluidic channel, viewed through the transparent window. The dashed box shows the walls of the channel. (ii) Contour plot of the refractive index as a function of the distance from the center of the width of the channel and of the distance along the length of the channel. The gradient of gray scale from black to white indicates values of the refractive index from 1.431 to 1.414. Only the main portion of the waveguide (1 cm x 0.005 cm, l x w) is simulated. (a–b *Adapted from Ref. 1.*)

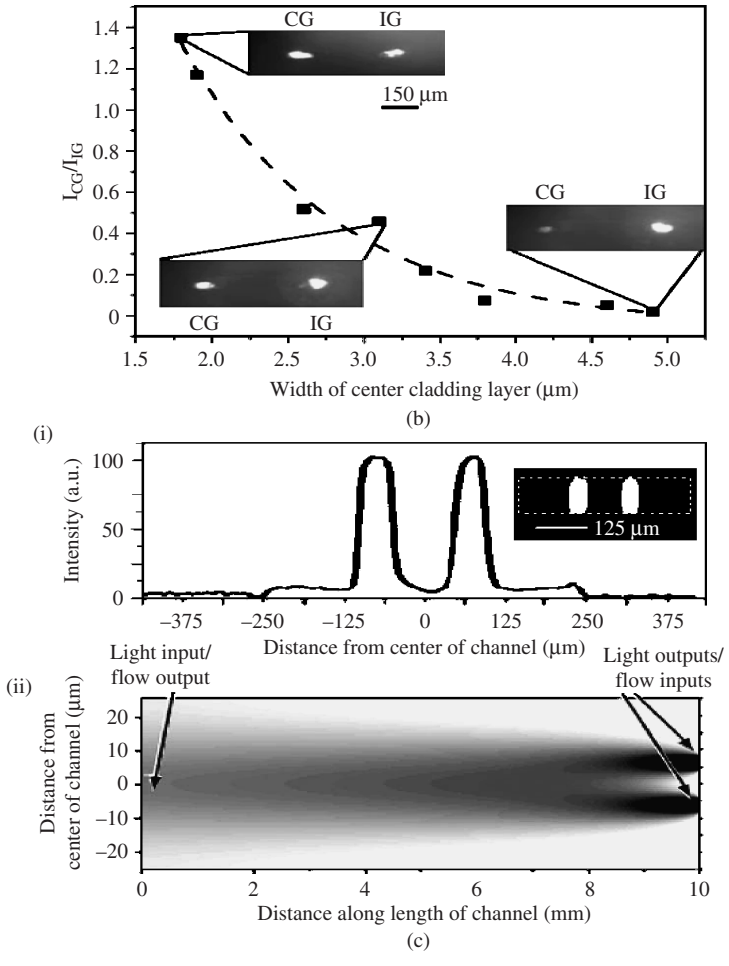

FIGURE 3-7 (*Continued*)

1. Optical Switch [1]: A L^2 waveguide is branched into three separate outlet channels. The relative rates of flow of the cladding liquids determine the path of the core liquid, and therefore the path of the guided light.
2. Evanescent-wave Coupler [1]: This device consists of two L^2 waveguides sharing an inner cladding stream with a width less than 5 μm. Light from an optical fiber is introduced into one of the L^2 waveguides. The rate of flow of the liquids adjusts the width of the inner cladding stream, and the efficiency of coupling of evanescent fields between the two cores of the L^2 waveguides. Efficient coupling is observed when the width of the inner cladding is below 2 μm.

Diffusion-controlled Splitter [10]

This device consists of two parallel L^2 waveguides. The rate of flow is sufficiently low to allow complete diffusive mixing of the liquids as they reach the end of the channel. As a result, the two core streams merge smoothly into a single L^2 waveguide. Light propagates in a direction opposite to that of the flow of liquids, that is, in the direction of decreasing extent of diffusive mixing. This system has been demonstrated to split a single input beam into two output beams with equal intensities.

Advantages and Disadvantages of L^2 Waveguides

To conclude our discussion of these systems, L^2 waveguides have two main advantages:

1. They are dynamically reconfigurable. Their structure and function depend on a continuous, laminar flow of the core and cladding liquids, and can therefore be reconfigured and adapted continuously in ways that are not possible with solid-state waveguides.
2. They are simple to fabricate. The roughness of the wall of the channel does not affect the smoothness of the laminar interface between the core and the cladding streams, and does not lead to the scattering of light or degradation in the performance of waveguides. L^2 waveguides can therefore be fabricated easily and rapidly in organic polymers by using the convenient techniques of rapid prototyping [11].

The L^2 waveguides also have prominent disadvantages:

1. A constant supply of fluids is necessary to maintain the waveguiding streams (a supply of 144 mL is necessary to run one stream at 100 μL/min for 24 h).
2. L^2 systems using water and PDMS are unable to guide light in the infrared (λ = 1300–1600 nm) used in telecommunications applications because of large absorptive losses in both the fluids and in the PDMS.
3. The speed of optical switching is ~ 0.1 Hz. This value is much slower than switching in conventional planar waveguides (~ 1–100 GHz). Nevertheless, the system should meet the demands of applications that do not require fast switching, such as optical sensing and bioassays.

3-5-2 L^2 Lenses

Design

The design of the L^2 lens is similar to that of the L^2 waveguide: it is formed by laminar flow of three streams of fluids; the index of

refraction of the central ("core") stream is higher than the index of the sandwiching ("cladding") streams [2]. The streams enter a microchannel containing an "expansion chamber"—a region in which the width of the channel expands laterally. Figure 3-8 shows a schematic diagram of this system. The expansion chamber is typically 10 times wider than its entrance and exit. For some rates of flow, the shape of the interface between the core and cladding streams in the expansion chamber is biconvex. This fluidic biconvex structure focuses light propagating in the plane of the expansion chamber, and perpendicular to the direction of flow of the liquids. By changing the relative rates of flow of the three streams, it is possible to change the curvature of the interface and thus the focal distance of the lens in real time.

To observe the focal point of the lens within the PDMS device (~ 2 cm × 2 cm), the contrast in refractive indices should be sufficiently large ($\Delta n_d > \sim 0.1$). Here, benzyl alcohol ($n_d = 1.54$) and benzothiazole ($n_d = 1.64$) have been used as the core liquid; and trifluoroethanol ($n_d = 1.29$) as the cladding. To facilitate beam tracing and determination of the focal point of the L^2 lens, an aperture can be included in front of the expansion chamber to block incident light from regions of the lens close to the inlet and outlet where the radius of curvature is highly nonuniform (Fig. 3-8). The aperture is formed

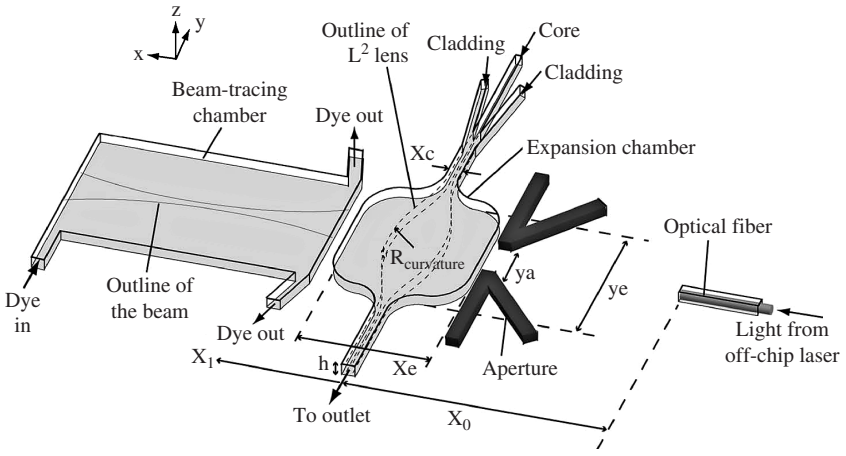

FIGURE 3-8 Schematic representation of the experimental setup for focusing light exiting an optical fiber through the liquid-core liquid-cladding (L^2) lens. The aperture is formed by two channels filled with black ink after fabrication. The channel for the formation of the L^2 lens contains a square expansion chamber. The solid lines show the walls of the channel, and the dashed lines show the interfaces between the core and the cladding streams. $R_{curvature}$ is the radius of curvature of this interface. The height (h) of the channel is about 100 mm. The beam-tracing chamber behind the L^2 lens is filled with solution of a fluorescent dye (2.5 μm Rhodamine 640 perchlorate in ethylene glycol) to make the optical path visible. (*Adapted from Ref. 2.*)

by filling two separate channels with black ink. For applications that require higher intensity at the focus, the aperture can be removed. In order to visualize the optical path, a beam-tracing chamber filled fluorescent dyes (2.5 μM rhodamine 640 perchlorate in ethylene glycol) is incorporated behind the L^2 lens.

Characterization

Figure 3-9 shows the shapes of the L^2 lens under different flow conditions. Since the height of the expansion chamber was much smaller than its width and length, the flow was quasi-two- dimensional, and the L^2 lens is roughly cylindrical. When the rates of flow of the left and the right cladding streams were the same, the core stream, or, the L^2 lens, was biconvex and symmetrical inside the expansion chamber. Varying the relative flow rates between the left and the right claddings varies the curvatures of the left and right interfaces separately. It is therefore possible to obtain an extensive range of lens shapes: meniscus, plano-convex, and biconvex.

The L^2 lens focused light; the FWHM (full width at half-maximum) of the beam at the focus achieved was ~ 16 μm, 20 times less than the initial beam width, using a 334-μm aperture. This beam size was limited by aberration due to the shape of the L^2 lens; the diffraction-limited width at the focal point is ~ 7 μm using this aperture. The enhancement factor (defined here as the ratio of the peak intensity of a focused beam to the intensity of an unfocused beam at the same point) achieved was 9 without any aperture (the enhancement factors were usually between 3 and 4 among previous works on microfabricated lenses).

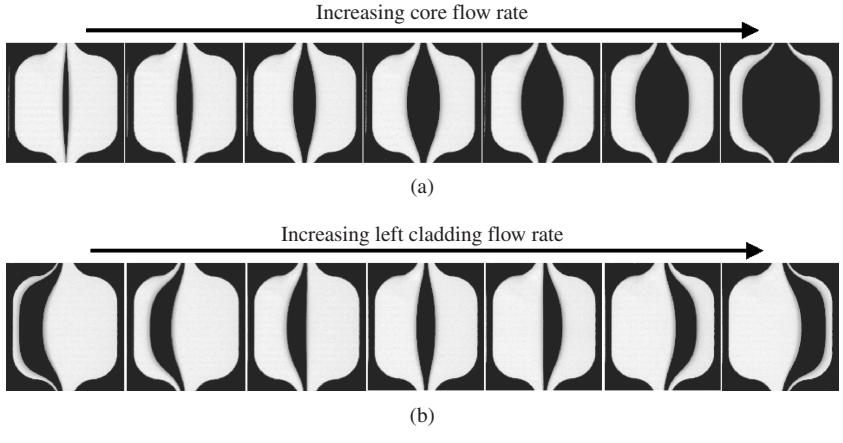

Figure 3-9 (a) Fluorescence images of the L^2 lens in the expansion chamber as the rate of flow of the core stream increases (from left to right). The cladding liquid was dyed to make it easily imaged; the dye was omitted in normal operation of the L^2 lens. (b) Fluorescence images of the L^2 lens as the rate of flow of the left cladding stream increases (from left to right).

Figure 3-10a shows the focal distance, measured from the center of the lens to the focal point, as a function of the core flow rate. The variation of the focal distance follows the variation of the curvature of the lens as expected from geometrical optics: a lens with a higher curvature focuses light at a shorter distance than one with a lower curvature. To achieve even shorter focal distances, one can use liquids with a larger contrast in refractive indices. Alternatively, one can use a smaller expansion chamber: at the same expansion ratio, the radius of curvature of the core-cladding interface is smaller in a smaller chamber; the focal distance achieved should also be shorter.

The beam-tracing chamber allows detailed analysis of the quality of the focused beam. Figure 3-10b and 3-10c compares the focused beam under the same flow conditions using a 500-μm-aperture and a 334-μm-aperture, respectively. The aberration of the L^2 lens was prominent in the former case: the areas of high light intensity were not limited to the paraxial focal point. This aberration is caused by the deviation of the shape of the core-cladding interface from the ideal lens shape. Making small adjustments to the shape of the expansion chamber and fine-tuning the shape of the lens should correct this aberration.

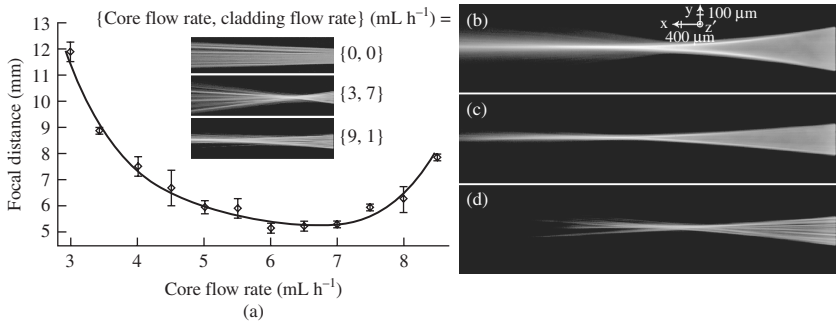

Figure 3-10 (a) Focal distance of the L^2 lens as a function of the rate of flow of the core stream. The core liquid was benzothiazole, and the cladding liquid was a mixture of ethylene glycol and ethanol with effective refractive index matched to that of PDMS. The total rate of flow of the core and cladding streams was fixed at 10 mL/h. The line is a guide to the eye only. The inset shows images of the focused beams in the beam-tracing chamber at the indicated flow rates. (b–d) Optical micrographs of the focused beam using (b) a 500-μm aperture, and (c) a 334-μm aperture, respectively. The core liquid was benzothiazole (n_d = 1.64) and the cladding liquid was a mixture of ethylene glycol and ethanol with effective refractive index matched to that of PDMS (n_d = 1.41). The core flow rate was 6 mL/h, and the cladding flow rate was 4 mL/h. Aberration was more prominent in (b) using a 500-μm aperture. (d) Optical micrograph of the focused beam using trifluoroethanol (n_d = 1.29) as the cladding liquid. The core liquid was benzothiazole. The aperture size was 334 μm. The core flow rate was 3 mL/h, and the cladding flow rate was 7 mL/h. Compared with (c), beam quality decreased due to the scattering of light at the PDMS-cladding interface. (*Adapted from Ref. 2.*)

Figure 3-10d shows the image of the focused beam using a L^2 lens with trifluoroethanol ($n_d = 1.29$) as the cladding liquid and benzothiazole as the core liquid. Due to the higher contrast in refractive index between the core and the cladding, the focal distance achieved was smaller. The quality of the beam was visibly worse than the case when the index of the cladding liquid was matched to that of PDMS (Fig. 3-10b and 3-10c). The streaks in the light beam were due to scattering of light from the rough channel wall.

3-5-3 L^2 Light Sources

We developed various on-chip fluidic light sources based on the L^2 waveguide systems for optical detection and spectroscopic analysis in integrated microanalytical systems (μTAS). In these systems, the liquid cores contain fluorescent dyes, excited by incident light from an external halogen bulb or a pump laser. Although external excitation sources are still necessary, integration of fluorescent light sources during device fabrication removes both the need for insertion and alignment of optical-fiber light sources and the constraints on channel size imposed by fiber optics.

Broadband Fluorescent Light Source

The construction of a microfluidic broadband light source is similar to that of a L^2 waveguide [12]. Solutions of multiple fluorescent dyes form the core streams, sandwiched by cladding streams with lower index of refraction. Excitation of these dyes by an external halogen bulb results in a broadband optical output with wavelength ranging from 450 to 750 nm.

Simultaneous use of multiple fluorophores in a common solution, in a single L^2 light source, is not possible, because of energy transfer from fluorophores emitting at shorter wavelength to fluorophores emitting at longer wavelength. Spatial separation of the fluorophores in different streams circumvents this problem. One design uses a cascade (series) of single-core, dye light sources of increasing absorption energy to generate a combined broadband output (Fig. 3-11a and 3-11b). The second approach uses a parallel array of single-core, dye light sources (Fig. 3-11c and 3-11d). The spectral content of the light output for both cascade and array light sources can be controlled through the choice of flow rates and dyes. Output intensity from these light sources is comparable to standard fiberoptic spectrophotometer light sources.

L^2 Microfluidic Dye Laser

Details about different microfluidic dye lasers can be found in Chap.10. Here we describe the use of L^2 waveguide for dye laser [13]. The construction of a microfluidic dye laser is similar to that of a L^2 waveguide. Solutions of fluorescent dye act as the gain media. They form the core streams, sandwiched by cladding streams with

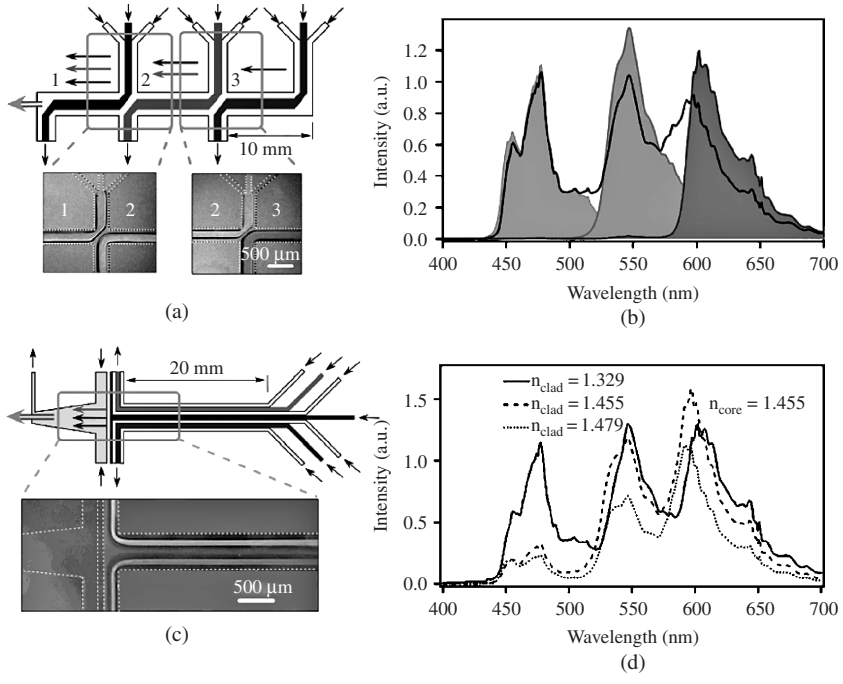

FIGURE 3-11 (a) Top-view scheme for a cascade of L^2 fluorescent light sources consisting of a series of microfluidic channels in PDMS. Multiple waveguides occupy the same central microfluidic channel. The flow of waveguide 2 displaces waveguide 3, and the flow of waveguide 1 displaces waveguide 2 at cross-junctions in the central channel. Light output is transferred between waveguides at these junctions where fluids take 90° turns. The dimensions of the central channel were 130 μm × 300 μm × 3 cm ($h \times w \times l$). Insets: Optical micrographs of the cross-junctions. The brightness and contrast have been adjusted for clarity. Dotted lines highlight the walls of the channels. (b) Spectral output (solid line) of a cascade of L^2 fluorescent light sources containing 0.5 mM solutions of perylene, fluorescein, and sulforhodamine B in DMSO/EG (1:1), when the entire central channel was irradiated with a single halogen source (uncollimated). Flow rates were 0.8, 2, and 5 mL/h for respective fluorescent cores (1, 2, and 3). Core/cladding rates were kept at a ratio of 2:1 for each waveguide. Selective illumination of discrete sections of the central microchannel with a collimated halogen source (each region of illumination was 4 mm in diameter) allowed selective excitation of individual fluorophores (shaded areas). (c) Top-view scheme for the array of L^2 fluorescent light sources, consisting of parallel L^2 waveguides in a single PDMS microchannel. An end-coupled, tapered, liquid-core waveguide filled with DMSO collected the total fluorescence output. Inset: Optical micrograph of the T-junction. Dotted lines outline the walls of the PDMS channels. (d) Spectral output (solid line) from an array of L^2 fluorescent light sources containing 0.5 mM solutions of perylene, fluorescein, and sulforhodamine B in DMSO/EG (1:1), with various cladding liquids: methanol ($n_{cladding} < n_{core}$); DMSO/EG (1:1, $n_{cladding} = n_{core}$); DMSO ($n_{cladding} > n_{core}$). Flow rates for all inputs were held constant at 4 mL/h each. (*Adapted from Ref. 12.*)

lower index of refraction, in a microchannel of length 5 to 20 mm where the dye is pumped optically by an external laser source. The microchannel terminates at both ends with T-junctions coated with thin layers of gold or silver to act as mirrors for the optical cavity (Fig. 3-12).

Lasing Characteristics

Lasing was demonstrated with 2-mM rhodamine 640 perchlorate in methanol as the core stream, and pure methanol as the cladding stream. A 532-nm pump laser beam (frequency doubled Nd:YAG, 50-Hz repetition rate, 16-ns pulse) is elongated and focused onto the microchannel with a cylindrical lens. A high rate of flow (~ 30 mL/h) is applied to ensure a rapid replenishment of the dye. Coupled with the short (16 ns) pulse length, potential photobleaching of the dyes is avoided at the power levels used (up to 0.15 mJ/pulse).

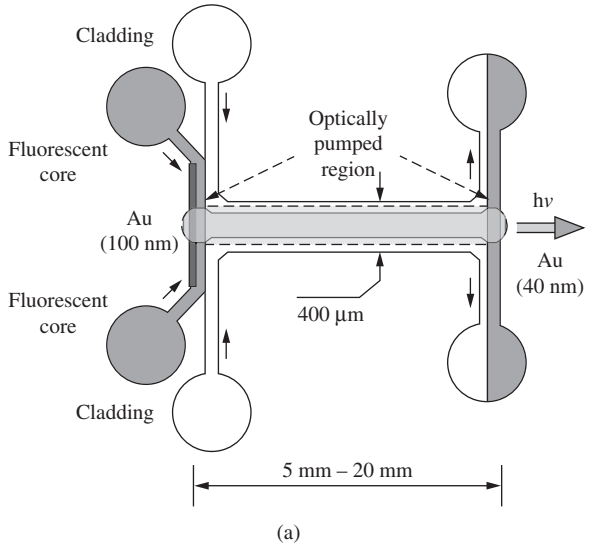

Figure 3-12 (a) Top-view scheme for a L^2 waveguide laser consisting of a liquid cladding and fluorescent liquid core flowing laminarly in a microfluidic channel in PDMS. The dimensions of the central channel were 100 mm × 400 mm × 10 mm (height × width × length). The 532-nm laser beam (frequency-doubled Nd:YAG, 50 Hz repetition rate, 16-ns pulse) was elongated with a cylindrical lens, and the optical pumping region covered the full length of the waveguiding region for the 10-mm-long channel. (b) Dependence of the intensity of the optical output and line width (FWHM) on the energy of the pump pulse. The curves are drawn to guide the eye. (c) Adjustment of the peak wavelength of the light output by changing the composition of the mixed methanol-DMSO liquid core with constant concentration of the dye (2 mM). (*Adapted from Ref. 13.*)

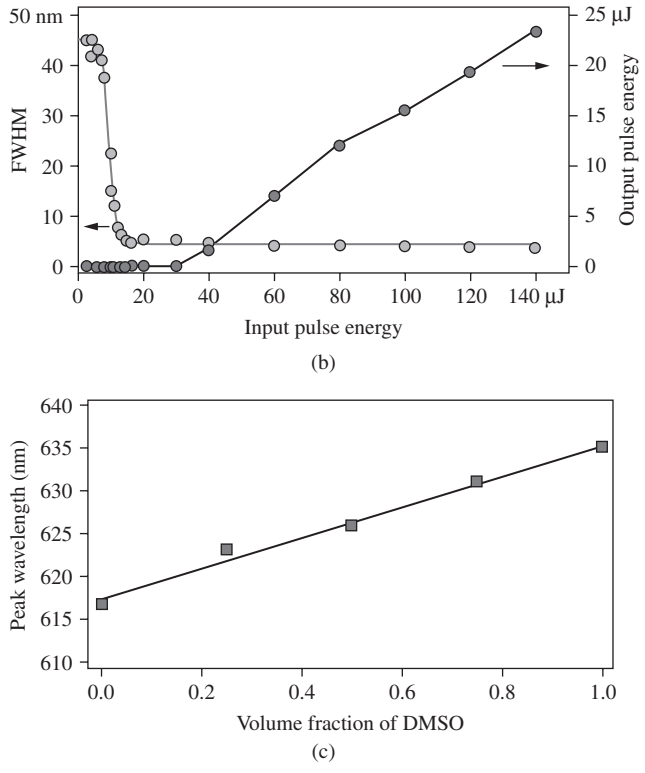

FIGURE 3-12 (*Continued*)

Figure 3-12b is a plot of output power and line width as a function of pump power. At low pump power (< 5 μJ/pulse) the line width (full width at half-maximum, FWHM) of the emission is ~ 45 nm, with λ_{max} centered at 625 nm. The line width drops to ~4 nm between pump powers of 7 and 16 μJ. The threshold for lasing occurs at 22 μJ pulse energy.

Wavelength Tunability

Like other dye lasers, the output wavelength can be changed by changing the choice and volume fraction of the solvent for the dye. Changing the solvent in the fluorescent core provides a simple way to adjust the wavelength of emission for a given dye without incorporating dispersive elements (prisms or gratings) into the optical cavity. For example, the wavelength of the light output for rhodamine 640 shifted by more than 20 nm by changing the composition of the core liquid; λ_{max} = 617 nm for methanol (MeOH), 631 nm for ethylene glycol, and 634 nm for dimethyl sulfoxide (DMSO). Adjusting

the composition of a mixture of DMSO and MeOH in the core allows continuous tuning of λ_{max} (Fig. 3-12c).

3-5-4 Bubble Grating

So far we have only focused on laminar systems using miscible fluids. Another interesting system involves the use of immiscible fluids to form emulsions and foams in microfluidic channels. These dispersions form periodic, self-assembled geometries that can also be reconfigured in real time by varying fluid properties and flow conditions. Here we describe a tunable, fluidic, two-dimensional diffraction grating based on a microfluidic system comprising a flow-focusing device for generating bubbles, and a flowing, regular lattice of bubbles formed by dynamic self-assembly [14].

As described in Chap. 1, the flow-focusing device consists of two inlet channels for the liquid phase, and a single inlet channel for the gaseous phase (Fig. 3-13a). The gas and liquid phases meet at a junction upstream of a narrow orifice. The gaseous thread periodically

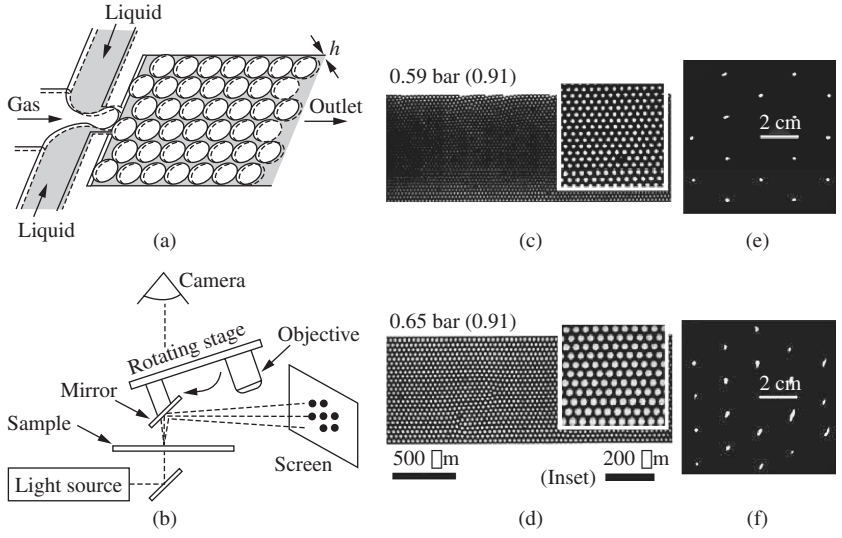

Figure 3-13 Schematic representations of the experimental setup. (a) The flow-focusing bubble generator and self-assembled lattice of bubbles. A tank of nitrogen gas connects to the gas inlet, and digitally controlled syringes connect to the liquid inlets. The system generates monodisperse bubbles that pack into a quasi two-dimensional sheet. (b) Diffraction and display of incident laser beam. Diffracted laser light orthogonal to the plane of bubble lattice is displayed on a white screen. (c–d) Packing of bubbles in a straight outlet channel that was 1-mm wide and 16-μm high. The rate of flow of the continuous phase was 0.028 μL/s. The numbers denote the input gas pressure and the volume fraction of bubbles (φ_{vol}) in parentheses. (c) 0.59 bar, $\varphi_{vol} = 0.91$, and (D) 0.65 bar, $\varphi_{vol} = 0.91$; their corresponding diffraction patterns are shown in (e) and (f) respectively. (*Adapted from Ref. 14.*)

enters the orifice, breaks, and releases a bubble into the outlet channel. As low gas pressures, the volume fraction (φ_{vol}) of the bubbles formed is low, and the bubbles flow in disordered packs. As φ_{vol} increases, the bubbles organize into hexagonally packed domains. As φ_{vol} approaches 0.91, the limit of packing of disks on the plane, the domains become a single lattice extending throughout the outlet channel. At $\varphi_{vol} \sim 0.91$, the bubbles fill the entire plane of the channel; the defects in the lattices are minimized.

Figure 3-13b shows the optical setup to characterize the diffraction patterns from the bubble lattices. A He/Ne laser ($\lambda = 632.8$ nm) illuminates the center of the bubble lattice. The direction of the beam is perpendicular to the plane of the device 1 cm downstream from the flow-focusing nozzle. Diffraction patterns are projected onto a white screen.

Figure 3-13c to 3-13f shows the bubble lattices and their corresponding diffraction patterns. These bubble lattice gratings can be modeled as both amplitude gratings and phase gratings. The menisci of the bubbles refract light radially, in a way that is similar to diffraction gratings formed from periodic arrays of dots or holes—that is, amplitude gratings. The bubbles and the carrying fluid also represent periodic arrays of alternating refractive indices—phase gratings. Changing the pressure of the gas and rate of flow of the liquid applied to the flow-focusing device changes the structure of the bubble lattices, and the diffraction patterns generated. The switching time is less than 10 s.

3-6 Conclusions

Dynamic optofluidic components based on liquid-liquid interfaces are simple to design, fabricate, and operate. They are adaptive and reconfigurable; the range of tuning is large, and only limited by the choice of liquids that can be injected into the microfluidic systems. Fluidic optical systems are also readily integrable with microanalytical and lab-on-a-chip systems for biochemical detection, where the analytes of interest are usually in the liquid phase.

The main disadvantage of these optofluidic components is the need for a constant supply of fluids. The range of refractive index available in fluids is also limited: the highest is around 1.75; this value is much lower than that in solids. They have limited transparency in the infrared, and are therefore mostly used in the visible region of the spectrum. In addition, the speed of optical switching is slow (on the order of seconds) compared to conventional optical devices. Nevertheless, these devices should still be useful for applications that do not require fast switching, such as optical sensing.

Optical systems based on liquid-liquid interfaces are still in their infancy of development. There are enough data to show that these

systems "work" optically: one can make optofluidic analogs of various familiar devices, such as waveguides and lenses; one can manipulate light in ways that cannot be accomplished using conventional solid-state devices. The question now is "Who cares?"

It is unlikely that this class of optofluidic devices will compete with conventional, solid-state devices in optical communications, where durability and stability are of paramount importance. Optofluidic systems seem, however, to be well suited for bioanalysis and lab-on-a-chip systems, where the samples are usually present in aqueous solutions, and where it is possible to use the strategy of cofabrication to generate multiple useful functions, from analysis and generation of light to the manipulation of particles using magnetic fields, in devices made using a single step of fabrication [15, 16]. A wide range of applications in biomedicine, food testing, environmental testing, biological research, drug testing, forensics, and homeland security all seem plausible.

Optics is an area that has followed a paradigm—solid-state fabrication focused on ultrahigh optical performance and durability, but with minimal adaptability. L^2 systems suggest another paradigm: systems that only function when they operate in dissipative mode—for example, with fluids flowing through them—and in which the systems are intrinsically unstable but highly adaptable. Time will tell the value of these characteristics.

References

1. D. B. Wolfe, R. S. Conroy, P. Garstecki, B. T. Mayers, M. A. Fischbach, K. E. Paul, M. Prentiss, and G. M. Whitesides, "Dynamic control of liquid-core/liquid-cladding optical waveguides," *Proc. Natl. Acad. Sci. U. S. A.*, 101, (2004), 12434–12438.
2. S. K. Y. Tang, C. A. Stan, and G. M. Whitesides, "Dynamically reconfigurable liquid-core liquid-cladding lens in a microfluidic channel," *Lab Chip*, 8, (2008), 395–401.
3. H. G. Elias, in *Polymer Handbook*, eds., J. Brandrup, E. H. Immergut, E. A. Grulke, A. Abe, and D. R. Bloch, Wiley-Interscience, (1999), New York, p. III 55–58
4. S. K. Y. Tang, B. T. Mayers, D. V. Vezenov, and G. M. Whitesides, "Optical waveguiding using thermal gradients across homogeneous liquids in microfluidic channels," *Appl. Phys. Lett.*, 88, (2006), 061112/061111–061112/061113.
5. R. S. Conroy, B. T. Mayers, D.V. Vezenov, D. B. Wolfe, M. G. Prentiss, and G. M. Whitesides, "Optical waveguiding in suspensions of dielectric particles," *Appl. Opt.*, 44, (2005), 7853–7857.
6. S. Y. Yang, J. J. Chieh, H. E. Horng, C.-Y. Hong, and H. C. Yang, "Origin and applications of magnetically tunable refractive index of magnetic fluid films," *Appl. Phys. Lett.*, 84, (2004), 5204–5206.
7. J. N. Lee, C. Park, and G. M. Whitesides, "Solvent compatibility of poly(dimethylsiloxane)-based microfluidic devices," *Anal. Chem.*, 75, (2003), 6544–6554.
8. M. Brady and C. Pozrikidis, "Diffusive transport across irregular and fractal walls," *Proc. R. Soc. London, Ser. A*, 442, (1993), 571–583.
9. T. Tamir, *Guided-Wave Optoelectronics*, Springer, New York, (1998).

10. D. B. Wolfe, D. V. Vezenov, B. T. Mayers, G. M. Whitesides, R. S. Conroy, and M. G. Prentiss, "Diffusion-controlled optical elements for optofluidics," *Appl. Phys. Lett.*, 87, (2005), 181105/181101–181105/181103.
11. J. C. McDonald and G. M. Whitesides, "Poly(dimethylsiloxane) as a Material for fabricating microfluidic devices," *Acc. Chem. Res.*, 35, (2002), 491–499.
12. B. T. Mayers, D. V. Vezenov, V. I. Vullev, and G. M. Whitesides, "Arrays and cascades of fluorescent liquid-liquid waveguides: broadband light sources for spectroscopy in microchannels," *Anal. Chem.*, 77, (2005), 1310–1316.
13. D. V. Vezenov, B. T. Mayers, R. S. Conroy, G. M. Whitesides, P. T. Snee, Y. Chan, D. G. Nocera, and M. G. Bawendi, "A low-threshold, high-efficiency microfluidic waveguide laser," *J. Am. Chem. Soc.*, 127, (2005), 8952–8953.
14. M. Hashimoto, B. Mayers, P. Garstecki, and G. M. Whitesides, "Flowing lattices of bubbles as tunable, self-assembled diffraction gratings," *Small*, 2, (2006), 1292–1298.
15. A. C. Siegel, S. S. Shevkoplyas, D. B. Weibel, D. A. Bruzewicz, A. W. Martinez, and G. M. Whitesides, "Cofabrication of electromagnets and microfluidic systems in poly(dimethylsiloxane)," *Angew. Chem., Int. Ed.*, 45, (2006), 6877–6882.
16. A. C. Siegel, D. A. Bruzewicz, D. B. Weibel, and G. M. Whitesides, "Microsolidics: fabrication of three-dimensional metallic microstructures in poly(dimethylsiloxane)," *Adv. Mater.*, 19, (2007) , 727–733.